Letter

Measurement of the cross sections for $e^+e^- \to \eta\pi^+\pi^-$ at center-of-mass energies between 2.00 and 3.08 GeV

M. Ablikim *et al.*[*]
(BESIII Collaboration)

(Received 17 October 2023; accepted 28 November 2023; published 19 December 2023)

Using data samples collected at center-of-mass energies between 2.000 and 3.080 GeV with the BESIII detector operating at the BEPCII collider, a partial-wave analysis is performed on the process $e^+e^- \to \eta\pi^+\pi^-$. In addition to the dominant $e^+e^- \to \rho\eta$ component, the $e^+e^- \to a_2(1320)\pi$ process is also sizable, contributing up to 24% of the total reaction. The measured cross sections of the process $e^+e^- \to \eta\pi^+\pi^-$ are systematically higher than those of *BABAR* by more than 3σ at center-of-mass energies between 2.000 and 2.300 GeV. In the cross section line shape for $e^+e^- \to a_2(1320)\pi$, a resonant structure is observed with a significance of 5.5σ, with $M = (2044 \pm 31 \pm 4)\ \mathrm{MeV}/c^2$, $\Gamma = (163 \pm 69 \pm 24)$ MeV, and $\mathcal{B}_{\mathcal{R}} \cdot \Gamma^{R}_{e^+e^-} = (34.6 \pm 17.1 \pm 6.0)$ eV or $(137.1 \pm 73.3 \pm 2.1)$ eV. In the cross section line shape for $e^+e^- \to \rho\eta$, an evidence of a dip structure around 2180 MeV/c^2 is observed with statistical significance of 3.0σ.

DOI: 10.1103/PhysRevD.108.L111101

Determining the hadronic contribution to the muon anomalous magnetic moment $(g_\mu - 2)$ is currently a high priority in hadronic physics. The latest measurement of $(g_\mu - 2)$ from Fermilab increased the tension between experiments and theories to a 5.0σ discrepancy [1,2], while recent lattice gauge theory predictions reduced this discrepancy [3]. The Standard Model (SM) calculation of $(g_\mu - 2)$ requires inputs from experimental e^+e^- hadronic cross section data to account for the hadronic vacuum polarization term. An updated SM calculation that considers all available hadronic data will likely yield a less significant discrepancy with experiment [1]. In the calculation, a sum of exclusive states must be used, in which the $e^+e^- \to \eta\pi^+\pi^-$ process has a sizable contribution [4–6]. Improved measurements of this process are therefore important to improve the reliability of the $(g_\mu - 2)$ calculation.

The process $e^+e^- \to \eta\pi^+\pi^-$ has previously been studied at energies from threshold to 3.5 GeV by several experiments: DM1 [7], ND [8], DM2 [9], CMD-2 [10], SND [11–13], *BABAR* [14,15], and CMD-3 [16]. In previous studies, the $e^+e^- \to \eta\pi^+\pi^-$ final state was simulated using only the $e^+e^- \to \rho\eta$ hadronic intermediate state, while other intermediate processes such as $e^+e^- \to a_2(1320)\pi$ were not considered in the determination of the efficiency.

The two-body processes $e^+e^- \to \rho\eta$ and $e^+e^- \to a_2(1320)\pi$ are important for the spectroscopy of the excited ρ-like states, including the $\rho(2000)$, $\rho(2150)$, and $\rho(2270)$. The $\rho(2000)$ was found in $p\bar{p}$ collisions [17,18] and has been explained as a radial excitation of the $\rho(1700)$ [18] and as a mixed state with a $^3D_1$ component [19,20]. Reference [20] indicates that $e^+e^- \to a_2(1320)\pi$ is a good channel for investigating $\rho(2000)$. The $\rho(2150)$ was initially regarded as a 2^3D_1 state [21] but was later considered to be a 4^3S_1 state [20,22–24]. The $\rho(2150)$ has been widely studied in e^+e^-, $p\bar{p}$, s-channel $N\bar{N}$, and πp experiments [25], but inconsistencies in the measured masses and widths make the $\rho(2150)$ more controversial. The $\rho(2270)$ was first observed in photoproduction [26] and categorized as a 3^3D_1 state [22,24]. Up to now there have been no published results on the production of the $\rho(2270)$ in e^+e^- collision experiments.

In this Letter, we present a partial-wave analysis (PWA) of the process $e^+e^- \to \eta\pi^+\pi^-$ using data collected with the BESIII detector. There are 19 datasets used in this analysis, with c.m. energies from 2.00 to 3.08 GeV and a total integrated luminosity of 648 pb^{-1}. The charge-conjugated processes are included by default in the following discussions.

The BESIII detector has a geometrical acceptance of 93% of the full solid angle and consists of four main components: (i) a small cell, helium-based multilayer drift chamber (MDC), (ii) a time-of-flight system made from two layers of plastic scintillator, (iii) an electromagnetic calorimeter (EMC) made of CsI(Tl) crystals, and (iv) a resistive plate chamber-based muon chamber. More details of the design and performance of the BESIII detector can be

---

[*] Full author list given at the end of the Letter.

found in Ref. [27]. The GEANT4 [28] based Monte Carlo (MC) simulation of the full detector is performed to optimize the event selection criteria, to understand potential backgrounds and to determine the detection efficiency. The signal MC samples are generated with CONEXC [29], which incorporates a higher-order initial state radiation (ISR) correction. The subsequent decay $\eta \to \gamma\gamma$ is simulated by BesEvtGen [30,31]. Inclusive MC samples equivalent to twice the datasets at $\sqrt{s} = 2.1250$, 2.396, and 2.900 GeV are generated, respectively, to study the backgrounds. The $e^+e^- \to (\gamma)e^+e^-, (\gamma)\mu^+\mu^-$, and $\gamma\gamma$ events are simulated with the BabaYaga generator [32], while $e^+e^- \to$ hadrons events are generated with a hybrid generator [29].

To identify $e^+e^- \to \eta\pi^+\pi^-$ candidates, final states with only one oppositely charged pion pair and at least two photons are selected. The selection criteria for charged tracks, particle identification (PID), and photons are the same as described in Ref. [33]. A vertex fit is imposed on the selected charged tracks to ensure that they originate from the same interaction point. The η meson is reconstructed with $\eta \to \gamma\gamma$. To suppress background due to the miscombination of photons, $\cos\theta_\gamma$ is required to be less than 0.95, where θ_γ is the polar angle of one photon in the helicity frame of the η meson. To further suppress the background, a four-constraint (4C) kinematic fit imposing energy-momentum conservation is employed, and $\chi^2_{4C} < 100$ is required. The Bhabha events are removed with the requirement of $E/p < 0.8$, where E is the deposited energy in the EMC and p is the momentum measured by the MDC for the charged pion. Based on an analysis of the inclusive MC events, the processes $e^+e^- \to \pi^+\pi^-\pi^0\pi^0$ and $e^+e^- \to \pi^+\pi^-\pi^0$ are found to be the dominant backgrounds, and no peaking background is observed. Signal candidates are required to be within the η mass signal region, which is defined as $[0.523, 0.573]$ GeV/c^2 on the photon pair invariant mass. The $M(\gamma\gamma)$ distribution at $\sqrt{s} = 2.125$ is shown in Fig. 1, and Fig. 1 of the Supplemental Material [34] shows the $M(\gamma\gamma)$ at $\sqrt{s} = 2.396$ and $\sqrt{s} = 2.900$ GeV. The events in the η mass sideband regions, which are defined as [0.478, 0.503] and $[0.593, 0.618]$ GeV/c^2, are used to estimate the background. The signal purities after sideband subtraction for different c.m. energies are listed in Table I of the Supplemental Material [34].

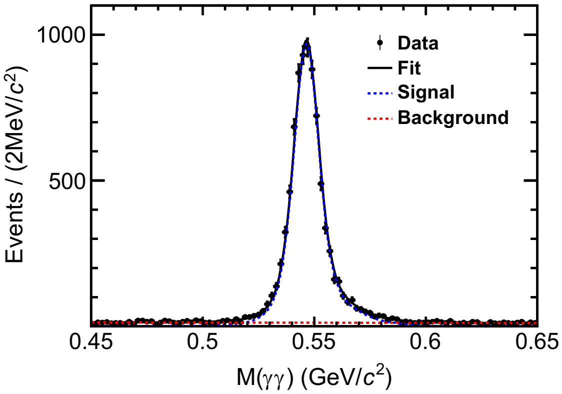

FIG. 1. Fit to the $M(\gamma\gamma)$ distribution at $\sqrt{s} = 2.125$ GeV. Dots with error bars are data, blue dashed line is the signal shape, red dashed line is the continuum background, the black line gives the total fit result.

To obtain a reliable efficiency for the process $e^+e^- \to \eta\pi^+\pi^-$ and to extract the contributions from the intermediate processes, a PWA based on the GPUPWA framework [35] is performed on the surviving candidate events. The quasi-two-body decay amplitudes in the sequential decay processes $e^+e^- \to \eta X$, $X \to \pi^+\pi^-$ and $e^+e^- \to \pi^+(\pi^-)X$, $X \to \pi^-(\pi^+)\eta$ are constructed using covariant tensor amplitudes [36]. The intermediate state X is parametrized by relativistic Breit-Wigner (BW) functions with constant widths, except for the wide $\rho(770)$, which is described by the Gounaris-Sakurai model [37]. The complex coefficients of the amplitudes (relative magnitudes and phases) of the individual intermediate processes are determined by performing an unbinned maximum likelihood fit using MINUIT [38]. The probability for the observed events is characterized by the measured four-momenta of the particles in the final state [39]. The joint probability for observing N events in the data samples is

$$\mathcal{L} \equiv \prod_{i=1}^{N} \frac{|\sum_X A_X(\xi_i)|^2 \epsilon(\xi_i)\Phi(\xi_i)}{\sigma'}, \tag{1}$$

where $A_X(\xi_i)$ is the amplitude corresponding to intermediate resonance X, $\epsilon(\xi_i)$ is the detection efficiency, $\Phi(\xi_i)$ is the standard element of phase space, and σ' is the normalization integral.

The fit procedure includes all possible intermediate states from the PDG [25] that satisfy J^{PC} conservation in the subsequent two-body decay. The likelihood contribution of background events is evaluated from the η sideband region. All possible amplitudes are tried in the fit, and only those with statistical significance larger than 5σ are retained. The statistical significance of amplitude is estimated by incorporating the change in log-likelihood as well as the degrees of freedom in the fits, where the corresponding amplitude can be included or not.

The above strategy is implemented individually on the datasets at $\sqrt{s} = 2.125$, 2.396, and 2.900 GeV, which are the datasets with the highest signal yields. The nominal solution is summarized in Table I. The masses and widths of the $\rho(770)$ and $a_2(1320)$ in the PWA fit are determined by scanning the likelihood value and are consistent with those in the PDG [25]. Since the contribution of other intermediate processes is relatively small, their masses and widths are fixed to the PDG values. The fit fractions of the intermediate states are also summarized in Table I. The comparisons of invariant mass spectra and angular distributions between data and the MC projections at

TABLE I. Statistical significances and fit fractions of possible intermediate processes at $\sqrt{s} = 2.125$, 2.396, and 2.900 GeV.

$\sqrt{s} = 2.125$ GeV			$\sqrt{s} = 2.396$ GeV			$\sqrt{s} = 2.900$ GeV		
Process	Significance (σ)	Fraction (%)	Process	Significance (σ)	Fraction (%)	Process	Significance (σ)	Fraction (%)
$\rho(770)\eta$	>20	58.0 ± 1.0	$\rho(770)\eta$	>20	69.5 ± 2.5	$\rho(770)\eta$	>20	66.8 ± 2.2
$a_2(1320)\pi$	>20	24.1 ± 0.8	$a_2(1320)\pi$	>20	13.0 ± 1.1	$a_2(1320)\pi$	>10	21.7 ± 2.1
$\rho(1450)\eta$	>10	1.8 ± 0.3	$\rho(1450)\eta$	5.1	1.0 ± 0.4	$\rho(1450)\eta$	>10	16.5 ± 0.4
$a_2(1700)\pi$	>10	2.0 ± 0.3	$\rho_3(1690)\eta$	9.7	2.5 ± 0.5	$\rho(1700)\eta$	6.5	2.1 ± 0.1
…	…	…	$a_2(1700)\pi$	6.8	2.7 ± 0.4	…	…	…
…	…	…	$\rho(1700)\eta$	5.8	1.9 ± 0.9	…	…	…

$\sqrt{s} = 2.125$, 2.396, and 2.900 GeV are shown in Figs. 2–4 of the Supplemental Material [34], respectively. The MC results are consistent with data within statistical uncertainties.

Due to limited statistics, the above optimization strategy is not performed for the other 16 data samples. Instead, the same intermediate components are used as those found to be necessary at nearby c.m. energy points with higher statistics. The same intermediates as $\sqrt{s} = 2.125$ GeV are used for the datasets with $\sqrt{s} = 2.000$, 2.050, 2.100, 2.150, 2.175, 2.200, and 2.232 GeV. While the same intermediates as $\sqrt{s} = 2.396$ GeV are used for datasets with $\sqrt{s} = 2.309$, 2.386, 2.644, and 2.646 GeV. The same processes as 2.900 GeV are used in the fits to the remaining datasets.

The cross section σ at each c.m. energy is determined as

$$\sigma = \frac{N^{\mathrm{obs}}}{\mathcal{L} \cdot \epsilon \cdot \mathcal{B} \cdot (1 + \delta^{\gamma})}, \tag{2}$$

where N^{obs} is the signal yield, $\mathcal{L}$ is the integrated luminosity of the dataset, and ϵ is the detection efficiency extracted from signal MC events which are generated with the generator derived from the PWA. $\mathcal{B}$ is the product of the relevant daughter branching fractions, i.e., $\mathcal{B} = \mathcal{B}(\eta \to \gamma\gamma) = 39.4\%$ for $e^+e^- \to \eta\pi^+\pi^-$, $\mathcal{B} = \mathcal{B}(\rho \to \pi\pi) \cdot \mathcal{B}(\eta \to \gamma\gamma) = 39.4\%$ for $e^+e^- \to \rho\eta$, and $\mathcal{B} = \mathcal{B}(a_2(1320) \to \eta\pi) \cdot \mathcal{B}(\eta \to \gamma\gamma) = 5.7\%$ for $e^+e^- \to a_2(1320)\pi$, and $(1 + \delta^{\gamma})$ is the ISR correction factor obtained from a QED calculation [29,40] and incorporating the input cross sections in this analysis, where iterations are performed until the measured cross section converges.

The signal yields for $e^+e^- \to \eta\pi^+\pi^-$ are extracted from a simultaneous unbinned maximum-likelihood fit to the $M(\gamma\gamma)$ spectra at each c.m. energy. The signal is described by an MC-simulated shape convolved with a Gaussian function, which is used to compensate for the differences in calibration and resolution between data and MC simulation. The parameters of the Gaussian function are free. A first-order Chebyshev polynomial is used to describe the background. Once the signal yields for $e^+e^- \to \eta\pi^+\pi^-$ are obtained, the signal yields for the intermediate processes of $e^+e^- \to \rho\eta$ and $e^+e^- \to a_2(1320)\pi$ are determined by using their fractions derived from the PWA.

Below 2.3 GeV, the measured cross sections for $e^+e^- \to \eta\pi^+\pi^-$ are systematically 30% higher than those of *BABAR*, as shown in Fig. 2. The resulting cross sections and related variables are listed in the Supplemental Material [34], separately for $e^+e^- \to \eta\pi^+\pi^-$ and its intermediate processes $e^+e^- \to \rho\eta$ and $e^+e^- \to a_2(1320)\pi$.

By implementing the same strategy described in Ref. [41], the following sources of systematic uncertainties on the measured cross sections are considered. The uncertainty associated with the integrated luminosity, detection efficiency and PID for charged track, and photon efficiency have been studied in Refs. [42–44]. The helix parameters of the simulated charged tracks are corrected to match the resolution [45], and the difference with and without correction is taken as the systematic uncertainty related to the 4C kinematic fit. The uncertainty regarding the ISR effect is obtained with the accuracy of the radiation function [46] and the contribution from the cross section line shape, which is estimated by varying the model parameters of the line shape fit as performed in Refs. [41,43]. The uncertainties originating from the E/p ratio and η helicity angle requirements are estimated by the control samples of $J/\psi \to \pi^+\pi^-\pi^0$ and

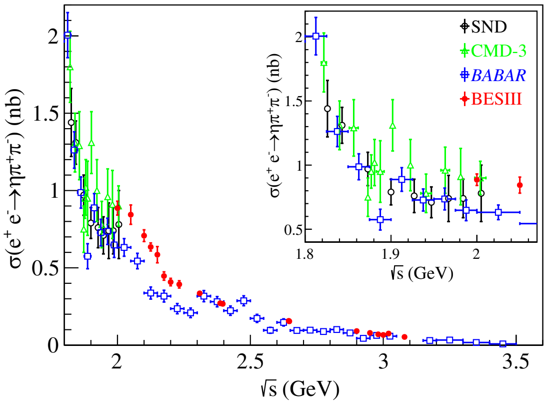

FIG. 2. Cross sections of $e^+e^- \to \eta\pi^+\pi^-$. Red solid dots with error bars are BESIII, blue hollow squares with error bars are *BABAR* [15], green hollow triangles with error bars are CMD-3 [16], and black hollow dots with error bars are SND [13]. The systematic uncertainties for BESIII are included.

$J/\psi \to K^+K^-\eta$, respectively. The uncertainties related to the fit procedure are investigated by varying the fit range, replacing the linear function for the background with a second-order polynomial function, and varying the width of the Gaussian function for the signal. The uncertainties from the branching fractions of intermediate states are taken from the PDG [25]. Uncertainty associated with the MC model for $e^+e^- \to \eta\pi^+\pi^-$ cross sections is estimated by the alternative PWA model including all the components with significance of more than 3σ.

The uncertainties due to the PWA fit mainly originate from the BW parametrization form, resonance parameters, extra resonances, barrier factor, and background estimation. The uncertainties from the BW parametrization are estimated by replacing the constant width in the relativistic BW function by a mass-dependent width. The uncertainties related to the resonance parameters, which are taken from the PDG and fixed in the nominal fit, are estimated by changing the mass and width by 1 standard deviation of the PDG values. The uncertainties associated with the extra resonances are estimated by alternative fits including all the components with significance greater than 3σ. The uncertainties regarding the barrier factor [47,48] are estimated by varying the radius of the centrifugal barrier by 1 standard deviation, assuming a uniform distribution of radius. The uncertainties from the background estimation originate from the background shape and the background fraction, which are estimated by using the lower or upper sideband events and varying the fraction by $\pm\sigma$, respectively. The resulting largest differences to the nominal result are assigned as the systematic uncertainties. The uncertainties from the PWA fit are strongly affected by the statistics. Thus, those uncertainties of data with $\sqrt{s} = 2.125$, $\sqrt{s} = 2.396$, and $\sqrt{s} = 2.900$ GeV are assigned to their nearby c.m. energies. Adding the systematic uncertainties in quadrature yields the total systematic uncertainties of about 3.9%–15.2% for different datasets, which are summarized in Table IV for $e^+e^- \to \eta\pi^+\pi^-$, Table V for $e^+e^- \to \rho\eta$, and Table VI for $e^+e^- \to a_2(1320)\pi$ in the Supplemental Material [34].

To investigate the possible structures in the measured cross sections of the quasi-two-body process $e^+e^- \to a_2(1320)\pi$, a χ^2 fit incorporating the correlated and uncorrelated uncertainties among different c.m. energies is performed. The fit probability density function is parametrized as the coherent sum of a continuum amplitude f_1 and a resonant amplitude f_2,

$$\sigma(s) = |f_1 + e^{i\phi} f_2|^2, \tag{3}$$

where ϕ is the relative phase angle between the amplitudes. The amplitude f_1 is written as

$$f_1 = C_0 \cdot s^{-n} \sqrt{\Phi(\sqrt{s})}, \tag{4}$$

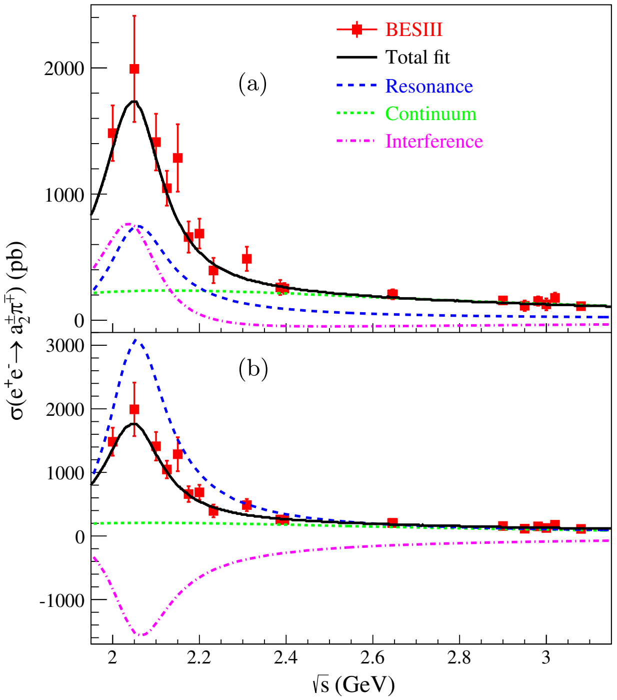

FIG. 3. Fits to the $e^+e^- \to a_2(1320)\pi$ cross sections. (a) Solution 1, constructive interference. (b) Solution 2, destructive interference. Solid squares with error bars are BESIII data. The black solid curve is the total fit result, the blue dashed line is the resonant component, the green dashed line is the continuum contribution, and the magenta dot-dashed line represents the interference between the resonance and the continuum contribution. The systematic uncertainties are included.

where $C_0 \cdot s^{-n}$ describes the energy-dependent cross section of the continuum, $\sqrt{\Phi(\sqrt{s})}$ is the two-body phase space, which takes the angular momentum and the width of the final state into account [36]. The resonant amplitude f_2 is described with a BW function as

$$f_2 = \frac{\sqrt{12\pi\Gamma_R^{ee} \cdot \mathcal{B}_R \Gamma_R^{\mathrm{tot}}}}{s - M_R^2 + iM_R \cdot \Gamma_R^{\mathrm{tot}}} \sqrt{\frac{\Phi(\sqrt{s})}{\Phi(M_R)}}, \tag{5}$$

where M_R, Γ_R^{ee}, and Γ_R^{tot} are the mass, partial width to e^+e^-, and total width of the assumed resonance R. $\mathcal{B}_R$ is the branching fraction for $R \to a_2(1320)\pi$.

TABLE II. Resonant parameters from the fit to $e^+e^- \to a_2(1320)\pi$ cross sections. The first uncertainty is statistical, and the second one is systematic.

Parameter	Solution 1	Solution 2
M_R (MeV/c^2)	$2044 \pm 31 \pm 4$	
Γ_{tot}^R (MeV)	$163 \pm 69 \pm 24$	
$\mathcal{B}_\mathcal{R}\Gamma_{e^+e^-}^R$ (eV)	$34.6 \pm 17.1 \pm 6.0$	$137.1 \pm 73.3 \pm 2.1$
ϕ (rad)	$1.95 \pm 0.97 \pm 0.06$	$4.35 \pm 0.48 \pm 0.43$

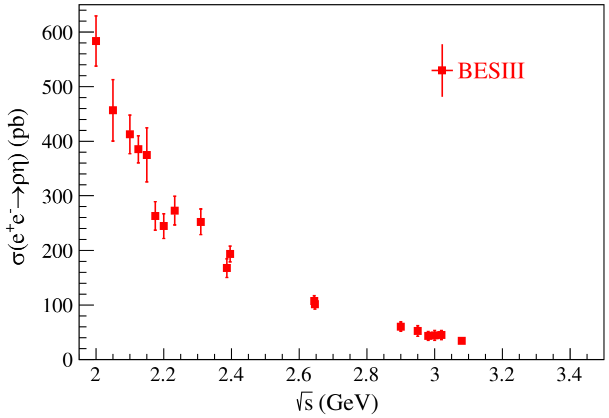

FIG. 4. Cross sections of $e^+e^- \to \rho\eta$. Solid squares with error bars are BESIII data.

Figure 3 shows the results of the fits to the cross sections for $e^+e^- \to a_2(1320)\pi$. There are two solutions with equal fit quality and identical mass and width for the resonance, while the product $\Gamma^{ee}_R \cdot \mathcal{B}_R$ and phase angle ϕ are different in the two solutions. The goodness of fit is $\chi^2/\text{n.d.f.} = 11.1/13 = 0.85$, where n.d.f. is the number of degrees of freedom. The fit parameters are summarized in Table II. The statistical significance of this resonance is estimated to be 5.5σ by comparing the change of χ^2 ($\Delta\chi^2 = 40.4$) with and without the R amplitude in the fit and taking the change of degrees of freedom ($\Delta\text{n.d.f.} = 4$) into account. The uncertainty of the parametrization of the continuum contribution for $e^+e^- \to a_2(1320)\pi$ is estimated by replacing the s-dependent continuum function C_1/s^n with an exponential function of the form $C_1 \cdot e^{-n(\sqrt{s}-M_{\text{th}})}$, where $M_{\text{th}} = m_{a_2} + m_\pi$. The differences of the obtained mass and width, which are 4 MeV$/c^2$ and 24 MeV, respectively, are taken as the systematic uncertainties.

Figure 4 shows the cross sections for $e^+e^- \to \rho\eta$. A dip structure around 2180 MeV$/c^2$ is observed with statistical significance of 3.0σ. Unfortunately, exploratory studies are not able to extract a physical resonance state. To make any conclusive statement, a finer energy scan is needed in this particular region.

In summary, we present a PWA of the process $e^+e^- \to \eta\pi^+\pi^-$ using data samples collected by the BESIII detector at 19 c.m. energies between 2.00 and 3.08 GeV. The cross sections for the process $e^+e^- \to \eta\pi^+\pi^-$ and its subprocesses $e^+e^- \to \rho\eta$ and $e^+e^- \to a_2(1320)\pi$ have been measured. The obtained cross sections of $e^+e^- \to \eta\pi^+\pi^-$ are systematically higher than those of *BABAR* [15] by more than 30% at $\sqrt{s}$ between 2.00 and 2.30 GeV. A coherent fit to the cross section line shape for the process $e^+e^- \to a_2(1320)\pi$ is performed using a resonant amplitude and a continuum amplitude. One resonant structure is observed with a significance of 5.5σ. Its mass, width, and $\mathcal{B}_{\mathcal{R}} \cdot \Gamma^R_{e^+e^-}$ are determined to be $(2044 \pm 31 \pm 4)$ MeV$/c^2$, $(163 \pm 69 \pm 24)$ MeV, and $(34.6 \pm 17.1 \pm 6.0)$ or $(137.1 \pm 73.3 \pm 2.1)$ eV, respectively. The observed structure agrees with the properties of the $\rho(2000)$ resonance observed in $e^+e^- \to \omega\pi^0$ [49], which indicates the first observation of the decay $\rho(2000) \to a_2(1320)\pi$. To further understand the dip structure around 2180 MeV$/c^2$ observed in the $e^+e^- \to \rho\eta$ cross section line shape, it will be necessary to acquire more energy points in order to improve the precision of the cross section measurements in the future.

The BESIII Collaboration thanks the staff of BEPCII and the IHEP computing center for their strong support. This work is supported in part by National Key R&D Program of China under Contracts No. 2023YFA1606000, No. 2020YFA0406400, No. 2020YFA0406300; National Natural Science Foundation of China (NSFC) under Contracts No. 11635010, No. 11735014, No. 11835012, No. 11935015, No. 11935016, No. 11935018, No. 11961141012, No. 12025502, No. 12035009, No. 12035013, No. 12061131003, No. 12192260, No. 12192261, No. 12192262, No. 12192263, No. 12192264, No. 12192265, No. 12221005, No. 12225509, No. 12235017, No. 12205255, No. 11975118; the Chinese Academy of Sciences (CAS) Large-Scale Scientific Facility Program; the CAS Center for Excellence in Particle Physics (CCEPP); Joint Large-Scale Scientific Facility Funds of the NSFC and CAS under Contracts No. U1832207, No. U1732263, No. U2032105; CAS Key Research Program of Frontier Sciences under Contracts No. QYZDJ-SSW-SLH003, No. QYZDJ-SSW-SLH040; 100 Talents Program of CAS; Natural Science Foundation of Gansu Province under Contract No. 23JRRA578; The Institute of Nuclear and Particle Physics (INPAC) and Shanghai Key Laboratory for Particle Physics and Cosmology; European Union's Horizon 2020 research and innovation program under Marie Sklodowska-Curie Grant Agreement under Contract No. 894790; German Research Foundation DFG under Contract No. 455635585, Collaborative Research Center CRC 1044, FOR5327, GRK 2149; Istituto Nazionale di Fisica Nucleare, Italy; Ministry of Development of Turkey under Contract No. DPT2006K-120470; National Research Foundation of Korea under Contract No. NRF-2022R1A2C1092335; National Science and Technology fund of Mongolia; National Science Research and Innovation Fund (NSRF) via the Program Management Unit for Human Resources & Institutional Development, Research and Innovation of Thailand under Contract No. B16F640076; Polish National Science Centre under Contract No. 2019/35/O/ST2/02907; The Swedish Research Council; U.S. Department of Energy under Award No. DE-FG02-05ER41374.

[1] D. P. Aguillard *et al.* (Muon $g-2$ Collaboration), Phys. Rev. Lett. **131**, 161802 (2023).

[2] T. Aoyama *et al.*, Phys. Rep. **887**, 1 (2020).

[3] S. Borsanyi *et al.*, Nature (London) **593**, 51 (2021).

[4] M. Davier, A. Hoecker, B. Malaescu, and Z. Zhang, Eur. Phys. J. C **77**, 827 (2017).

[5] F. Jegerlehner, Acta Phys. Pol. B **49**, 1157 (2018).

[6] A. Keshavarzi, D. Nomura, and T. Teubner, Phys. Rev. D **97**, 114025 (2018).

[7] A. Cordier, B. Delcourt, P. Eschstruth, F. Fulda, G. Grosdidier, J. Jeanjean, M. Jeanjean, R. Madaras, J. Masnou, J. Perez Y Jorba, A. Quenzer, M. Ribes, F. Rumpf, J. Bertrand, and J. Bizot, Nucl. Phys. **B172**, 13 (1980).

[8] V. Druzhinin, M. Dubrovin, S. Eidelman, V. Golubev, V. Ivanchenko, A. Lysenko, E. Pakhtusova, A. Peryshkin, A. Polunin, S. Serednyakov, V. Sidorov, Y. Shatunov, and A. Skrinsky, Phys. Lett. B **174**, 115 (1986).

[9] A. Antonelli *et al.* (DM2 Collaboration), Phys. Lett. B **212**, 133 (1988).

[10] R. R. Akhmetshin *et al.* (CMD-2 Collaboration), Phys. Lett. B **489**, 125 (2000).

[11] M. N. Achasov *et al.*, JETP Lett. **92**, 80 (2010).

[12] V. M. Aulchenko *et al.* (SND Collaboration), Phys. Rev. D **91**, 052013 (2015).

[13] M. N. Achasov *et al.*, Phys. Rev. D **97**, 012008 (2018).

[14] B. Aubert *et al.* (*BABAR* Collaboration), Phys. Rev. D **76**, 092005 (2007); **77**, 119902(E) (2008).

[15] J. P. Lees *et al.* (*BABAR* Collaboration), Phys. Rev. D **97**, 052007 (2018).

[16] S. S. Gribanov *et al.*, J. High Energy Phys. 01 (2020) 112.

[17] A. Hasan and D. V. Bugg, Phys. Lett. B **334**, 215 (1994).

[18] A. V. Anisovich, C. A. Baker, C. J. Batty, D. V. Bugg, L. Montanet, V. A. Nikonov, A. V. Sarantsev, V. V. Sarantsev, and B. S. Zou, Phys. Lett. B **542**, 8 (2002).

[19] D. V. Bugg, Phys. Rep. **397**, 257 (2004).

[20] Z.-Y. Li, D.-M. Li, E. Wang, W.-C. Yan, and Q.-T. Song, Phys. Rev. D **104**, 034013 (2021).

[21] S. Godfrey and N. Isgur, Phys. Rev. D **32**, 189 (1985).

[22] D. V. Bugg, Phys. Rev. D **87**, 118501 (2013).

[23] P. Masjuan, E. Ruiz Arriola, and W. Broniowski, Phys. Rev. D **87**, 118502 (2013).

[24] L.-P. He, X. Wang, and X. Liu, Phys. Rev. D **88**, 034008 (2013).

[25] R. L. Workman *et al.* (Particle Data Group), Prog. Theor. Exp. Phys. **2022**, 083C01 (2022).

[26] M. Atkinson *et al.* (Omega Photon Collaboration), Z. Phys. C **29**, 333 (1985).

[27] M. Ablikim *et al.* (BESIII Collaboration), Nucl. Instrum. Methods Phys. Res., Sect. A **614**, 345 (2010).

[28] S. Agostinelli *et al.* (GEANT4 Collaboration), Nucl. Instrum. Methods Phys. Res., Sect. A **506**, 250 (2003).

[29] R.-G. Ping *et al.*, Chin. Phys. C **40**, 113002 (2016).

[30] D. J. Lange, Nucl. Instrum. Methods Phys. Res., Sect. A **462**, 152 (2001).

[31] R.-G. Ping, Chin. Phys. C **32**, 599 (2008).

[32] G. Balossini, C. M. Carloni Calame, G. Montagna, O. Nicrosini, and F. Piccinini, Nucl. Phys. **B758**, 227 (2006).

[33] M. Ablikim *et al.* (BESIII Collaboration), Phys. Rev. D **103**, 072007 (2021).

[34] See Supplemental Material at http://link.aps.org/supplemental/10.1103/PhysRevD.108.L111101 for a summary of the number of signal events, luminosity, cross section and systematic uncertainty at each energy point, the comparison of invariant mass spectra and angular distribution between data, and fit results at $\sqrt{s} = 2.125$, 2.396, and 2.900 GeV.

[35] N. Berger, B. Liu, and J. Wang, J. Phys. Conf. Ser. **219**, 042031 (2010).

[36] B. S. Zou and D. V. Bugg, Eur. Phys. J. A **16**, 537 (2003).

[37] G. J. Gounaris and J. J. Sakurai, Phys. Rev. Lett. **21**, 244 (1968).

[38] F. James and M. Roos, Comput. Phys. Commun. **10**, 343 (1975).

[39] M. Ablikim *et al.* (BESIII Collaboration), Phys. Rev. D **87**, 032008 (2013).

[40] E. A. Kuraev and V. S. Fadin, Sov. J. Nucl. Phys. **41**, 466 (1985), https://inspirehep.net/literature/217313.

[41] M. Ablikim *et al.* (BESIII Collaboration), Phys. Rev. Lett. **124**, 112001 (2020).

[42] M. Ablikim *et al.* (BESIII Collaboration), Chin. Phys. C **41**, 063001 (2017).

[43] M. Ablikim *et al.* (BESIII Collaboration), Phys. Rev. D **99**, 032001 (2019).

[44] M. Ablikim *et al.* (BESIII Collaboration), Phys. Rev. D **99**, 011101 (2019).

[45] M. Ablikim *et al.* (BESIII Collaboration), Phys. Rev. D **87**, 012002 (2013).

[46] S. Actis *et al.* (Working Group on Radiative Corrections, Monte Carlo Generators for Low Energies Collaboration), Eur. Phys. J. C **66**, 585 (2010).

[47] S. U. Chung, Phys. Rev. D **48**, 1225 (1993); **56**, 4419(E) (1997).

[48] F. Von Hippel and C. Quigg, Phys. Rev. D **5**, 624 (1972).

[49] M. Ablikim *et al.* (BESIII Collaboration), Phys. Lett. B **813**, 136059 (2021).

M. Ablikim,[1] M. N. Achasov,[4,b] P. Adlarson,[75] X. C. Ai,[80] R. Aliberti,[35] A. Amoroso,[74a,74c] M. R. An,[39] Q. An,[71,58] Y. Bai,[57]
O. Bakina,[36] I. Balossino,[29a] Y. Ban,[46,g] H.-R. Bao,[63] V. Batozskaya,[1,44] K. Begzsuren,[32] N. Berger,[35] M. Berlowski,[44]
M. Bertani,[28a] D. Bettoni,[29a] F. Bianchi,[74a,74c] E. Bianco,[74a,74c] A. Bortone,[74a,74c] I. Boyko,[36] R. A. Briere,[5]
A. Brueggemann,[68] H. Cai,[76] X. Cai,[1,58] A. Calcaterra,[28a] G. F. Cao,[1,63] N. Cao,[1,63] S. A. Cetin,[62a] J. F. Chang,[1,58]
W. L. Chang,[1,63] G. R. Che,[43] G. Chelkov,[36,a] C. Chen,[43] Chao Chen,[55] G. Chen,[1] H. S. Chen,[1,63] M. L. Chen,[1,58,63]
S. J. Chen,[42] S. L. Chen,[45] S. M. Chen,[61] T. Chen,[1,63] X. R. Chen,[31,63] X. T. Chen,[1,63] Y. B. Chen,[1,58] Y. Q. Chen,[34]
Z. J. Chen,[25,h] S. K. Choi,[10] X. Chu,[43] G. Cibinetto,[29a] S. C. Coen,[3] F. Cossio,[74c] J. J. Cui,[50] H. L. Dai,[1,58] J. P. Dai,[78]

A. Dbeyssi,[18] R. E. de Boer,[3] D. Dedovich,[36] Z. Y. Deng,[1] A. Denig,[35] I. Denysenko,[36] M. Destefanis,[74a,74c] F. De Mori,[74a,74c] B. Ding,[66,1] X. X. Ding,[46,g] Y. Ding,[34] Y. Ding,[40] J. Dong,[1,58] L. Y. Dong,[1,63] M. Y. Dong,[1,58,63] X. Dong,[76] M. C. Du,[1] S. X. Du,[80] Z. H. Duan,[42] P. Egorov,[36,a] Y. H. Fan,[45] J. Fang,[1,58] S. S. Fang,[1,63] W. X. Fang,[1] Y. Fang,[1] Y. Q. Fang,[1,58] R. Farinelli,[29a] L. Fava,[74b,74c] F. Feldbauer,[3] G. Felici,[28a] C. Q. Feng,[71,58] J. H. Feng,[59] Y. T. Feng,[71] K. Fischer,[69] M. Fritsch,[3] C. D. Fu,[1] J. L. Fu,[63] Y. W. Fu,[1] H. Gao,[63] Y. N. Gao,[46,g] Yang Gao,[71,58] S. Garbolino,[74c] I. Garzia,[29a,29b] P. T. Ge,[76] Z. W. Ge,[42] C. Geng,[59] E. M. Gersabeck,[67] A. Gilman,[69] K. Goetzen,[13] L. Gong,[40] W. X. Gong,[1,58] W. Gradl,[35] S. Gramigna,[29a,29b] M. Greco,[74a,74c] M. H. Gu,[1,58] Y. T. Gu,[15] C. Y. Guan,[1,63] Z. L. Guan,[22] A. Q. Guo,[31,63] L. B. Guo,[41] M. J. Guo,[50] R. P. Guo,[49] Y. P. Guo,[12,f] A. Guskov,[36,a] J. Gutierrez,[27] K. L. Han,[63] T. T. Han,[1] W. Y. Han,[39] X. Q. Hao,[19] F. A. Harris,[65] K. K. He,[55] K. L. He,[1,63] F. H. H. Heinsius,[3] C. H. Heinz,[35] Y. K. Heng,[1,58,63] C. Herold,[60] T. Holtmann,[3] P. C. Hong,[12,f] G. Y. Hou,[1,63] X. T. Hou,[1,63] Y. R. Hou,[63] Z. L. Hou,[1] B. Y. Hu,[59] H. M. Hu,[1,63] J. F. Hu,[56,i] T. Hu,[1,58,63] Y. Hu,[1] G. S. Huang,[71,58] K. X. Huang,[59] L. Q. Huang,[31,63] X. T. Huang,[50] Y. P. Huang,[1] T. Hussain,[73] N. Hüsken,[27,35] N. in der Wiesche,[68] M. Irshad,[71,58] J. Jackson,[27] S. Jaeger,[3] S. Janchiv,[32] J. H. Jeong,[10] Q. Ji,[1] Q. P. Ji,[19] X. B. Ji,[1,63] X. L. Ji,[1,58] Y. Y. Ji,[50] X. Q. Jia,[50] Z. K. Jia,[71,58] H. B. Jiang,[76] P. C. Jiang,[46,g] S. S. Jiang,[39] T. J. Jiang,[16] X. S. Jiang,[1,58,63] Y. Jiang,[63] J. B. Jiao,[50] Z. Jiao,[23] S. Jin,[42] Y. Jin,[66] M. Q. Jing,[1,63] X. M. Jing,[63] T. Johansson,[75] X. Kui,[1] S. Kabana,[33] N. Kalantar-Nayestanaki,[64] X. L. Kang,[9] X. S. Kang,[40] M. Kavatsyuk,[64] B. C. Ke,[80] V. Khachatryan,[27] A. Khoukaz,[68] R. Kiuchi,[1] O. B. Kolcu,[62a] B. Kopf,[3] M. Kuessner,[3] A. Kupsc,[44,75] W. Kühn,[37] J. J. Lane,[67] P. Larin,[18] L. Lavezzi,[74a,74c] T. T. Lei,[71,58] Z. H. Lei,[71,58] H. Leithoff,[35] M. Lellmann,[35] T. Lenz,[35] C. Li,[47] C. Li,[43] C. H. Li,[39] Cheng Li,[71,58] D. M. Li,[80] F. Li,[1,58] G. Li,[1] H. Li,[71,58] H. B. Li,[1,63] H. J. Li,[19] H. N. Li,[56,i] Hui Li,[43] J. R. Li,[61] J. S. Li,[59] J. W. Li,[50] Ke Li,[1] L. J. Li,[1,63] L. K. Li,[1] Lei Li,[48] M. H. Li,[43] P. R. Li,[38,k] Q. X. Li,[50] S. X. Li,[12] T. Li,[50] W. D. Li,[1,63] W. G. Li,[1] X. H. Li,[71,58] X. L. Li,[50] Xiaoyu Li,[1,63] Y. G. Li,[46,g] Z. J. Li,[59] Z. X. Li,[15] C. Liang,[42] H. Liang,[1,63] H. Liang,[71,58] Y. F. Liang,[54] Y. T. Liang,[31,63] G. R. Liao,[14] L. Z. Liao,[50] Y. P. Liao,[1,63] J. Libby,[26] A. Limphirat,[60] D. X. Lin,[31,63] T. Lin,[1] B. J. Liu,[1] B. X. Liu,[76] C. Liu,[34] C. X. Liu,[1] F. H. Liu,[53] Fang Liu,[1] Feng Liu,[6] G. M. Liu,[56,i] H. Liu,[38,j,k] H. B. Liu,[15] H. M. Liu,[1,63] Huanhuan Liu,[1] Huihui Liu,[21] J. B. Liu,[71,58] J. Y. Liu,[1,63] K. Liu,[38,j,k] K. Y. Liu,[40] Ke Liu,[22] L. Liu,[71,58] L. C. Liu,[43] Lu Liu,[43] M. H. Liu,[12,f] P. L. Liu,[1] Q. Liu,[63] S. B. Liu,[71,58] T. Liu,[12,f] W. K. Liu,[43] W. M. Liu,[71,58] X. Liu,[38,j,k] Y. Liu,[80] Y. Liu,[38,j,k] Y. B. Liu,[43] Z. A. Liu,[1,58,63] Z. Q. Liu,[50] X. C. Lou,[1,58,63] F. X. Lu,[59] H. J. Lu,[23] J. G. Lu,[1,58] X. L. Lu,[1] Y. Lu,[7] Y. P. Lu,[1,58] Z. H. Lu,[1,63] C. L. Luo,[41] M. X. Luo,[79] T. Luo,[12,f] X. L. Luo,[1,58] X. R. Lyu,[63] Y. F. Lyu,[43] F. C. Ma,[40] H. Ma,[78] H. L. Ma,[1] J. L. Ma,[1,63] L. L. Ma,[50] M. M. Ma,[1,63] Q. M. Ma,[1] R. Q. Ma,[1,63] X. Y. Ma,[1,58] Y. Ma,[46,g] Y. M. Ma,[31] F. E. Maas,[18] M. Maggiora,[74a,74c] S. Malde,[69] Q. A. Malik,[73] A. Mangoni,[28b] Y. J. Mao,[46,g] Z. P. Mao,[1] S. Marcello,[74a,74c] Z. X. Meng,[66] J. G. Messchendorp,[13,64] G. Mezzadri,[29a] H. Miao,[1,63] T. J. Min,[42] R. E. Mitchell,[27] X. H. Mo,[1,58,63] B. Moses,[27] N. Yu. Muchnoi,[4,b] J. Muskalla,[35] Y. Nefedov,[36] F. Nerling,[18,d] I. B. Nikolaev,[4,b] Z. Ning,[1,58] S. Nisar,[11,l] Q. L. Niu,[38,j,k] W. D. Niu,[55] Y. Niu,[50] S. L. Olsen,[63] Q. Ouyang,[1,58,63] S. Pacetti,[28b,28c] X. Pan,[55] Y. Pan,[57] A. Pathak,[34] P. Patteri,[28a] Y. P. Pei,[71,58] M. Pelizaeus,[3] H. P. Peng,[71,58] Y. Y. Peng,[38,j,k] K. Peters,[13,d] J. L. Ping,[41] R. G. Ping,[1,63] S. Plura,[35] V. Prasad,[33] F. Z. Qi,[1] H. Qi,[71,58] H. R. Qi,[61] M. Qi,[42] T. Y. Qi,[12,f] S. Qian,[1,58] W. B. Qian,[63] C. F. Qiao,[63] J. J. Qin,[72] L. Q. Qin,[14] X. S. Qin,[50] Z. H. Qin,[1,58] J. F. Qiu,[1] S. Q. Qu,[61] C. F. Redmer,[35] K. J. Ren,[39] A. Rivetti,[74c] M. Rolo,[74c] G. Rong,[1,63] Ch. Rosner,[18] S. N. Ruan,[43] N. Salone,[44] A. Sarantsev,[36,c] Y. Schelhaas,[35] K. Schoenning,[75] M. Scodeggio,[29a,29b] K. Y. Shan,[12,f] W. Shan,[24] X. Y. Shan,[71,58] J. F. Shangguan,[55] L. G. Shao,[1,63] M. Shao,[71,58] C. P. Shen,[12,f] H. F. Shen,[1,63] W. H. Shen,[63] X. Y. Shen,[1,63] B. A. Shi,[63] H. C. Shi,[71,58] J. L. Shi,[12] J. Y. Shi,[1] Q. Q. Shi,[55] R. S. Shi,[1,63] X. Shi,[1,58] J. J. Song,[19] T. Z. Song,[59] W. M. Song,[34,1] Y. J. Song,[12] S. Sosio,[74a,74c] S. Spataro,[74a,74c] F. Stieler,[35] Y. J. Su,[63] G. B. Sun,[76] G. X. Sun,[1] H. Sun,[63] H. K. Sun,[1] J. F. Sun,[19] K. Sun,[61] L. Sun,[76] S. S. Sun,[1,63] T. Sun,[51,e] W. Y. Sun,[34] Y. Sun,[9] Y. J. Sun,[71,58] Y. Z. Sun,[1] Z. T. Sun,[50] Y. X. Tan,[71,58] C. J. Tang,[54] G. Y. Tang,[1] J. Tang,[59] Y. A. Tang,[76] L. Y. Tao,[72] Q. T. Tao,[25,h] M. Tat,[69] J. X. Teng,[71,58] V. Thoren,[75] W. H. Tian,[52] W. H. Tian,[59] Y. Tian,[31,63] Z. F. Tian,[76] I. Uman,[62b] Y. Wan,[55] S. J. Wang,[50] B. Wang,[1] B. L. Wang,[63] Bo Wang,[71,58] C. W. Wang,[42] D. Y. Wang,[46,g] F. Wang,[72] H. J. Wang,[38,j,k] J. P. Wang,[50] K. Wang,[1,58] L. L. Wang,[1] M. Wang,[50] Meng Wang,[1,63] N. Y. Wang,[63] S. Wang,[38,j,k] S. Wang,[12,f] T. Wang,[12,f] T. J. Wang,[43] W. Wang,[59] W. Wang,[72] W. P. Wang,[71,58] X. Wang,[46,g] X. F. Wang,[38,j,k] X. J. Wang,[39] X. L. Wang,[12,f] Y. Wang,[61] Y. D. Wang,[45] Y. F. Wang,[1,58,63] Y. L. Wang,[19] Y. N. Wang,[45] Y. Q. Wang,[1] Yaqian Wang,[17,1] Yi Wang,[61] Z. Wang,[1,58] Z. L. Wang,[72] Z. Y. Wang,[1,63] Ziyi Wang,[63] D. Wei,[70] D. H. Wei,[14] F. Weidner,[68] S. P. Wen,[1] C. W. Wenzel,[3] U. Wiedner,[3] G. Wilkinson,[69] M. Wolke,[75] L. Wollenberg,[3] C. Wu,[39] J. F. Wu,[1,8] L. H. Wu,[1] L. J. Wu,[1,63] X. Wu,[12,f] X. H. Wu,[34] Y. Wu,[71] Y. H. Wu,[55] Y. J. Wu,[31] Z. Wu,[1,58] L. Xia,[71,58] X. M. Xian,[39] T. Xiang,[46,g] D. Xiao,[38,j,k] G. Y. Xiao,[42] S. Y. Xiao,[1] Y. L. Xiao,[12,f] Z. J. Xiao,[41] C. Xie,[42] X. H. Xie,[46,g] Y. Xie,[50] Y. G. Xie,[1,58] Y. H. Xie,[6] Z. P. Xie,[71,58] T. Y. Xing,[1,63] C. F. Xu,[1,63] C. J. Xu,[59]

G. F. Xu,[1] H. Y. Xu,[66] Q. J. Xu,[16] Q. N. Xu,[30] W. Xu,[1] W. L. Xu,[66] X. P. Xu,[55] Y. C. Xu,[77] Z. P. Xu,[42] Z. S. Xu,[63] F. Yan,[12,f] L. Yan,[12,f] W. B. Yan,[71,58] W. C. Yan,[80] X. Q. Yan,[1] H. J. Yang,[51,e] H. L. Yang,[34] H. X. Yang,[1] Tao Yang,[1] Y. Yang,[12,f] Y. F. Yang,[43] Y. X. Yang,[1,63] Yifan Yang,[1,63] Z. W. Yang,[38,j,k] Z. P. Yao,[50] M. Ye,[1,58] M. H. Ye,[8] J. H. Yin,[1] Z. Y. You,[59] B. X. Yu,[1,58,63] C. X. Yu,[43] G. Yu,[1,63] J. S. Yu,[25,h] T. Yu,[72] X. D. Yu,[46,g] C. Z. Yuan,[1,63] L. Yuan,[2] S. C. Yuan,[1] Y. Yuan,[1,63] Z. Y. Yuan,[59] C. X. Yue,[39] A. A. Zafar,[73] F. R. Zeng,[50] S. H. Zeng,[72] X. Zeng,[12,f] Y. Zeng,[25,h] Y. J. Zeng,[1,63] X. Y. Zhai,[34] Y. C. Zhai,[50] Y. H. Zhan,[59] A. Q. Zhang,[1,63] B. L. Zhang,[1,63] B. X. Zhang,[1] D. H. Zhang,[43] G. Y. Zhang,[19] H. Zhang,[71] H. C. Zhang,[1,58,63] H. H. Zhang,[59] H. H. Zhang,[34] H. Q. Zhang,[1,58,63] H. Y. Zhang,[1,58] J. Zhang,[59] J. Zhang,[80] J. J. Zhang,[52] J. L. Zhang,[20] J. Q. Zhang,[41] J. W. Zhang,[1,58,63] J. X. Zhang,[38,j,k] J. Y. Zhang,[1] J. Z. Zhang,[1,63] Jianyu Zhang,[63] L. M. Zhang,[61] L. Q. Zhang,[59] Lei Zhang,[42] P. Zhang,[1,63] Q. Y. Zhang,[39,80] Shuihan Zhang,[1,63] Shulei Zhang,[25,h] X. D. Zhang,[45] X. M. Zhang,[1] X. Y. Zhang,[50] Y. Zhang,[69] Y. Zhang,[72] Y. T. Zhang,[80] Y. H. Zhang,[1,58] Yan Zhang,[71,58] Yao Zhang,[1] Z. D. Zhang,[1] Z. H. Zhang,[1] Z. L. Zhang,[34] Z. Y. Zhang,[76] Z. Y. Zhang,[43] G. Zhao,[1] J. Y. Zhao,[1,63] J. Z. Zhao,[1,58] Lei Zhao,[71,58] Ling Zhao,[1] M. G. Zhao,[43] R. P. Zhao,[63] S. J. Zhao,[80] Y. B. Zhao,[1,58] Y. X. Zhao,[31,63] Z. G. Zhao,[71,58] A. Zhemchugov,[36,a] B. Zheng,[72] J. P. Zheng,[1,58] W. J. Zheng,[1,63] Y. H. Zheng,[63] B. Zhong,[41] X. Zhong,[59] H. Zhou,[50] L. P. Zhou,[1,63] X. Zhou,[76] X. K. Zhou,[6] X. R. Zhou,[71,58] X. Y. Zhou,[39] Y. Z. Zhou,[12,f] J. Zhu,[43] K. Zhu,[1] K. J. Zhu,[1,58,63] L. Zhu,[34] L. X. Zhu,[63] S. H. Zhu,[70] S. Q. Zhu,[42] T. J. Zhu,[12,f] W. J. Zhu,[12,f] Y. C. Zhu,[71,58] Z. A. Zhu,[1,63] J. H. Zou,[1] and J. Zu[71,58]

(BESIII Collaboration)

[1]*Institute of High Energy Physics, Beijing 100049, People's Republic of China*
[2]*Beihang University, Beijing 100191, People's Republic of China*
[3]*Bochum Ruhr-University, D-44780 Bochum, Germany*
[4]*Budker Institute of Nuclear Physics SB RAS (BINP), Novosibirsk 630090, Russia*
[5]*Carnegie Mellon University, Pittsburgh, Pennsylvania 15213, USA*
[6]*Central China Normal University, Wuhan 430079, People's Republic of China*
[7]*Central South University, Changsha 410083, People's Republic of China*
[8]*China Center of Advanced Science and Technology, Beijing 100190, People's Republic of China*
[9]*China University of Geosciences, Wuhan 430074, People's Republic of China*
[10]*Chung-Ang University, Seoul 06974, Republic of Korea*
[11]*COMSATS University Islamabad, Lahore Campus, Defence Road, Off Raiwind Road, 54000 Lahore, Pakistan*
[12]*Fudan University, Shanghai 200433, People's Republic of China*
[13]*GSI Helmholtzcentre for Heavy Ion Research GmbH, D-64291 Darmstadt, Germany*
[14]*Guangxi Normal University, Guilin 541004, People's Republic of China*
[15]*Guangxi University, Nanning 530004, People's Republic of China*
[16]*Hangzhou Normal University, Hangzhou 310036, People's Republic of China*
[17]*Hebei University, Baoding 071002, People's Republic of China*
[18]*Helmholtz Institute Mainz, Staudinger Weg 18, D-55099 Mainz, Germany*
[19]*Henan Normal University, Xinxiang 453007, People's Republic of China*
[20]*Henan University, Kaifeng 475004, People's Republic of China*
[21]*Henan University of Science and Technology, Luoyang 471003, People's Republic of China*
[22]*Henan University of Technology, Zhengzhou 450001, People's Republic of China*
[23]*Huangshan College, Huangshan 245000, People's Republic of China*
[24]*Hunan Normal University, Changsha 410081, People's Republic of China*
[25]*Hunan University, Changsha 410082, People's Republic of China*
[26]*Indian Institute of Technology Madras, Chennai 600036, India*
[27]*Indiana University, Bloomington, Indiana 47405, USA*
[28a]*INFN Laboratori Nazionali di Frascati, I-00044, Frascati, Italy*
[28b]*INFN Sezione di Perugia, I-06100, Perugia, Italy*
[28c]*University of Perugia, I-06100, Perugia, Italy*
[29a]*INFN Sezione di Ferrara, I-44122, Ferrara, Italy*
[29b]*University of Ferrara, I-44122, Ferrara, Italy*
[30]*Inner Mongolia University, Hohhot 010021, People's Republic of China*
[31]*Institute of Modern Physics, Lanzhou 730000, People's Republic of China*
[32]*Institute of Physics and Technology, Peace Avenue 54B, Ulaanbaatar 13330, Mongolia*
[33]*Instituto de Alta Investigación, Universidad de Tarapacá, Casilla 7D, Arica 1000000, Chile*

[34]*Jilin University, Changchun 130012, People's Republic of China*
[35]*Johannes Gutenberg University of Mainz, Johann-Joachim-Becher-Weg 45, D-55099 Mainz, Germany*
[36]*Joint Institute for Nuclear Research, 141980 Dubna, Moscow region, Russia*
[37]*Justus-Liebig-Universitaet Giessen, II. Physikalisches Institut,*
Heinrich-Buff-Ring 16, D-35392 Giessen, Germany
[38]*Lanzhou University, Lanzhou 730000, People's Republic of China*
[39]*Liaoning Normal University, Dalian 116029, People's Republic of China*
[40]*Liaoning University, Shenyang 110036, People's Republic of China*
[41]*Nanjing Normal University, Nanjing 210023, People's Republic of China*
[42]*Nanjing University, Nanjing 210093, People's Republic of China*
[43]*Nankai University, Tianjin 300071, People's Republic of China*
[44]*National Centre for Nuclear Research, Warsaw 02-093, Poland*
[45]*North China Electric Power University, Beijing 102206, People's Republic of China*
[46]*Peking University, Beijing 100871, People's Republic of China*
[47]*Qufu Normal University, Qufu 273165, People's Republic of China*
[48]*Renmin University of China, Beijing 100872, People's Republic of China*
[49]*Shandong Normal University, Jinan 250014, People's Republic of China*
[50]*Shandong University, Jinan 250100, People's Republic of China*
[51]*Shanghai Jiao Tong University, Shanghai 200240, People's Republic of China*
[52]*Shanxi Normal University, Linfen 041004, People's Republic of China*
[53]*Shanxi University, Taiyuan 030006, People's Republic of China*
[54]*Sichuan University, Chengdu 610064, People's Republic of China*
[55]*Soochow University, Suzhou 215006, People's Republic of China*
[56]*South China Normal University, Guangzhou 510006, People's Republic of China*
[57]*Southeast University, Nanjing 211100, People's Republic of China*
[58]*State Key Laboratory of Particle Detection and Electronics,*
Beijing 100049, Hefei 230026, People's Republic of China
[59]*Sun Yat-Sen University, Guangzhou 510275, People's Republic of China*
[60]*Suranaree University of Technology, University Avenue 111, Nakhon Ratchasima 30000, Thailand*
[61]*Tsinghua University, Beijing 100084, People's Republic of China*
[62a]*Turkish Accelerator Center Particle Factory Group, Istinye University, 34010, Istanbul, Turkey*
[62b]*Near East University, Nicosia, North Cyprus, 99138, Mersin 10, Turkey*
[63]*University of Chinese Academy of Sciences, Beijing 100049, People's Republic of China*
[64]*University of Groningen, NL-9747 AA Groningen, The Netherlands*
[65]*University of Hawaii, Honolulu, Hawaii 96822, USA*
[66]*University of Jinan, Jinan 250022, People's Republic of China*
[67]*University of Manchester, Oxford Road, Manchester M13 9PL, United Kingdom*
[68]*University of Muenster, Wilhelm-Klemm-Strasse 9, 48149 Muenster, Germany*
[69]*University of Oxford, Keble Road, Oxford OX13RH, United Kingdom*
[70]*University of Science and Technology Liaoning, Anshan 114051, People's Republic of China*
[71]*University of Science and Technology of China, Hefei 230026, People's Republic of China*
[72]*University of South China, Hengyang 421001, People's Republic of China*
[73]*University of the Punjab, Lahore-54590, Pakistan*
[74a]*University of Turin, I-10125 Turin, Italy*
[74b]*University of Eastern Piedmont, I-15121 Alessandria, Italy*
[74c]*INFN, I-10125 Turin, Italy*
[75]*Uppsala University, Box 516, SE-75120 Uppsala, Sweden*
[76]*Wuhan University, Wuhan 430072, People's Republic of China*
[77]*Yantai University, Yantai 264005, People's Republic of China*
[78]*Yunnan University, Kunming 650500, People's Republic of China*
[79]*Zhejiang University, Hangzhou 310027, People's Republic of China*
[80]*Zhengzhou University, Zhengzhou 450001, People's Republic of China*

[a] Also at the Moscow Institute of Physics and Technology, Moscow 141700, Russia.
[b] Also at the Novosibirsk State University, Novosibirsk 630090, Russia.
[c] Also at the NRC "Kurchatov Institute," PNPI, 188300 Gatchina, Russia.
[d] Also at Goethe University Frankfurt, 60323 Frankfurt am Main, Germany.
[e] Also at Key Laboratory for Particle Physics, Astrophysics and Cosmology, Ministry of Education; Shanghai Key Laboratory for Particle Physics and Cosmology; Institute of Nuclear and Particle Physics, Shanghai 200240, People's Republic of China.

[f] Also at Key Laboratory of Nuclear Physics and Ion-beam Application (MOE) and Institute of Modern Physics, Fudan University, Shanghai 200443, People's Republic of China.
[g] Also at State Key Laboratory of Nuclear Physics and Technology, Peking University, Beijing 100871, People's Republic of China.
[h] Also at School of Physics and Electronics, Hunan University, Changsha 410082, China.
[i] Also at Guangdong Provincial Key Laboratory of Nuclear Science, Institute of Quantum Matter, South China Normal University, Guangzhou 510006, China.
[j] Also at MOE Frontiers Science Center for Rare Isotopes, Lanzhou University, Lanzhou 730000, People's Republic of China.
[k] Also at Lanzhou Center for Theoretical Physics, Lanzhou University, Lanzhou 730000, People's Republic of China.
[l] Also at the Department of Mathematical Sciences, IBA, Karachi 75270, Pakistan.